ISSN 2075-1133, Inorganic Materials: Applied Research, 2024, Vol. 15, No. 3, pp. 675–685. © Pleiades Publishing, Ltd., 2024.
Russian Text © The Author(s), 2023, published in Fizika i Khimiya Obrabotki Materialov, 2023, No. 3, pp. 18–32.

PLASMOCHEMICAL METHODS OF PRODUCTION AND TREATMENT OF MATERIALS

Oxidation of Zirconium Alloyed with Chromium Atoms by Means of Impact of Compression Plasma Flows

V. I. Shymanski[a, *], V. V. Sheveleva[a], V. V. Uglov[a], V. M. Astashynski[b], and A. M. Kuzmitski[b]

[a] *Belarusian State University, Minsk, 220030 Belarus*

[b] *Luikov Heat and Mass Transfer Institute, National Academy of Science of Belarus, Minsk, 220072 Belarus*

**e-mail: shymanskiv@mail.ru*

Received June 11, 2022; revised October 7, 2022; accepted December 20, 2022

Abstract—The results of studies on the zirconium crystal structure after initial stages of oxidation in an open air at temperature of 700°C for 15 min are presented. Samples of commercial pure zirconium with a minimal content of impurity atoms as well as chromium-alloyed zirconium have been studied by means of the action of compression plasma flows. The possibility of alloying the zirconium near-surface layer with chromium, with a chromium coating thickness of 1 μm, by means of compression plasma flows with the absorbed energy density of 25–43 J/cm^2 has been demonstrated. Stabilization of the high-temperature zirconium β phase in the form of β-Zr(Cr) solid solution and intermediate martensite α'-Zr phase has been observed. After isothermal annealing of zirconium samples at $T = 700$°C and irradiated with plasma flow with $Q_{max} = 43$ J/cm^2, no effect of the surface layer alloying with chromium atoms has been observed owing to its intense evaporation and ablation in the course of surface heating by plasma flow, as well as increased resistance to high-temperature oxidation at the initial stages in comparison with the initial state.

Keywords: zirconium, chromium, surface layer alloying, compression plasma flows, oxidation, zirconium oxide

DOI: 10.1134/S2075113324700096

INTRODUCTION

Zirconium and zirconium-based alloys are important structural materials for nuclear technology used in the manufacture of fuel element claddings in view of their low cross section of thermal neutron capture and high corrosion resistance. In order to increase the safety level of existing nuclear power plants and those under construction, special attention is paid to the structure and physical and mechanical properties of zirconium alloys, which are continuously improved by developing new compositions and modifying the structural-phase state of the surface. Zirconium alloys used in operating conditions at nuclear power plants are exposed to high levels of radiation, thermal, mechanical, and corrosive loads. An urgent problem is investigation of the behavior of the claddings of fuel elements made from zirconium alloys in the case of loss-of-coolant accident (LOCA), in which intense high-temperature oxidation occurs (700–1200°C) [1–6]. The formation of an oxide layer on the zirconium surface occurs within a few minutes and is accompanied by active high-temperature hydrogenation, which promotes the formation of embrittling zirconium hydrides. Thus, intensely occurring structural changes in the fuel rod material lead to its rapid destruction and the release of radioactive fission products outside the core, which does not allow operators of nuclear power plants to complete the process of bringing the reactor into a safe mode. Therefore, the development of methods for increasing the zirconium corrosion resistance from high-temperature oxidation is an urgent task.

A similar problem can be solved by creating a protective coating on the surface of zirconium preventing its active oxidation [7–9]. But this approach significantly changes the cross section for the thermal neutrons capture on the surface and leads to a decrease in the efficiency of the installation. Modification of the structural state of the near-surface layer, including an insignificant addition of an alloying element, may be an alternative method. At present, a very promising method for modifying the structural-phase state of a near-surface layer is a pulsed high-energy action on the surface by beams of charged particles (electrons, ions) or plasma flows. A number of experimental works [10–15] performed on many industrial alloys showed a significant increase in the physical and mechanical properties of their near-surface layers due to the microstructure dispersity, an increase in the degree of defectiveness, and the formation of inclusions of metastable phases after pulsed high-energy action.

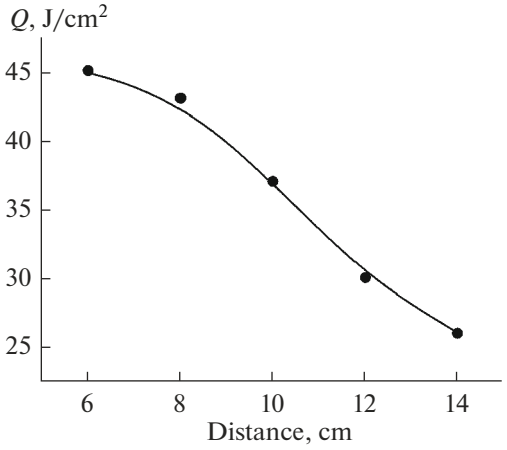

Fig. 1. Dependence of the absorbed energy density on the distance between the sample and the electrode at the capacitor voltage $U = 4.0$ kV.

The possibility of using high-energy pulsed compression plasma flows (CPFs) generated by quasi-stationary plasma accelerators [16–18] is considered in the present work. The influence of the CPF makes it possible to impart a sufficiently high energy density to the material surface layer (absorbed energy density reaches 70–100 J/cm^2) for an extended period of time exceeding 100 μs, which together increases the role of liquid-phase processes in a molten surface layer. In addition to changing the structural state of zirconium, doping with small concentrations of chromium atoms which can be realized in a single cycle under plasma exposure is proposed in the work. Since liquid-phase mixing is a high-speed hydrodynamic process that is not subjected to any thermodynamic restrictions, the number of embedded alloying atoms in the substrate of base metal can significantly exceed the equilibrium limit of their solubility. In addition, currently, the problem of using chromium to increase the corrosion resistance of zirconium alloys in various environments is actively studied [19–21]. Therefore, the choice of a technically pure zirconium alloy as a model material with a minimum content of impurities is due to the need to study the influence of both crystallization conditions under pulsed plasma exposure and alloying directly with chromium atoms on structural transformations, without taking into account other alloying elements often used in industrial alloys. Thus, the work sets the task of studying the fundamental principles of structural-phase transformations in zirconium in combination with alloying with chromium, high-speed crystallization, and subsequent oxidation.

The purpose of the work is to study the effect of plasma action on the alloying of the surface of zirconium with chromium atoms and the structural-phase changes that occur at the initial stages of oxidation.

EXPERMENTAL

Plates of technically pure zirconium alloy with a minimal amount of impurities (0.8 at % Hf, 0.9 at % Al, balance Zr), with dimensions of 5 × 10 mm and a thickness of 2 mm, on the surface of which a chromium coating with a thickness of ~ 1 μμm was applied by vacuum arc deposition, were used as the objects of investigations. The formed zirconium–chromium system was exposed to compression plasma flows in a magnetic-plasma compressor of compact geometry in an atmosphere of residual nitrogen gas. The residual atmosphere pressure was 1.33 kPa (10 Torr). The energy of the plasma flow was determined by the energy stored in a system of storage capacitors charged to a voltage of $U = 4.0$ kV. The discharge of the capacitors led to the formation of gas-discharge plasma between the electrodes in the chamber of the magnetoplasma compressor. The samples were placed in the compressor chamber at distances L from 8 to 14 cm from the electrode cuts, which made it possible to change the energy density absorbed by the surface layer of the sample. By calorimetric investigations, it was established that the selected range of changes in L made it possible to change the absorbed energy density Q from 43 to 25 J/cm^2, which was sufficient to melt the chromium coating and the near-surface layer of zirconium (Fig. 1).

The duration of the CPF pulse was 100 μs. At the selected distances from the electrodes, the plasma flow in a cross section has a diameter of 2–3 cm, which exceeds the area of the samples and allows us to assume a uniform effect of the plasma flow on the surface with each pulse. In order to exclude accidental deviations in the movement of the plasma flow, irradiation was carried out with three consecutive pulses, following each other with an interval of 10–15 s.

The samples were annealed in a muffle furnace at atmospheric pressure and a temperature of 700°C to study the oxidation kinetics of modified zirconium samples, as well as the structural and phase changes that occur. The accuracy of maintaining the temperature in the furnace was ±10°C. Studies of the initial stages of sample oxidation were carried out at short annealing times (no more than 15 min). The samples were cooled in air at room temperature. The choice of annealing temperatures was determined by the study of oxygen diffusion processes under conditions close to those during LOCA-type accidents. Of course, the chosen oxidation temperature corresponds to the minimal threshold achieved during LOCA-type accidents, which allows us to consider structural transformations in alloys at their initial stages. The oxidation kinetics of plasma-modified zirconium alloys doped with chromium atoms was studied on the basis of the weight gain associated with oxygen accumulation. To measure the mass of oxidized samples, a Radwag analytical balance was used, the accuracy of which was ±0.00005 g.

The phase composition of the samples was determined using X-ray diffraction analysis on an Ultima IV Rigaku diffractometer in the geometry of parallel beams in CuK_α radiation ($\lambda = 0.154178$ nm). X-ray diffraction patterns were recorded in the range of diffraction angles from 20° to 80° with a step of 0.05° at a detector speed of 2°/min. The surface morphology of the samples was studied using a LEO 1455 VP scanning electron microscope operating in the mode of recording both secondary and reflected electrons at an accelerating voltage of 20 kV. The elemental composition of the near-surface layer was determined on the basis of X-ray spectral microanalysis using an Oxford MaxN attachment to a scanning electron microscope.

RESULTS AND DISCUSSION

Structural-Phase State of Zirconium Alloyed with Chromium

When the CPF is exposed to the surface of a zirconium sample, part of the energy of the plasma flow is transferred to the surface layer, the main part of which is thermal energy and contributes to heating the sample. The features of structural changes in the irradiated material are determined by the ratio of the maximum achievable temperature and its melting point. In the case where heating occurs above the melting point, subsequent cooling involves a phase transition from the liquid to the solid phase and more significant changes in the structural state of the crystallized material. Therefore, such modes of plasma exposure were chosen that made it possible to ensure the density of absorbed energy that is necessary for melting the surface layer. The process of energy transfer from the plasma flow to the material can be described as follows. At the first stage of interaction, a sharp evaporation of atoms from the target surface occurs, which cannot be removed far from it and scattered in the compressor chamber owing to the compressive effect of the plasma flow, which holds the gas state (shock-compressed layer) near the surface. Namely, it is through this layer that energy is subsequently transferred from the target plasma flow owing to thermal conductivity. At the end of the pulse, 100 μs after the start of the discharge, the temperature on the surface reaches its maximum value, and the target substance is in a molten state. After this, the plasma flow begins to lose stability and the shock-compressed layer dissipates in the chamber. Hydrodynamic instabilities are generated on the free surface of the melt, which lead to an increase in disturbances at the boundary between the free surface of the melt and the environment, which are the main cause of hydrodynamic flows occurring in the molten part of the target.

Figure 2 shows images of the surface of zirconium samples obtained by scanning electron microscopy, which demonstrate a characteristic developed wavelike relief (Fig. 2a), which is absent on the sample in the initial state, and the formation of which is caused by the rapid crystallization of the disturbed surface held by surface tension forces. With increasing energy of the plasma flow, the characteristic period of such disturbances on the surface decreases, and the amplitude of the waviness increases. The characteristic period of the wavelike surface relief increases from 25 μm (at $Q = 25$ J/cm^2) to 70 μm (at $Q = 43$ J/cm^2). Apparently, with an increase in the density of absorbed energy during the same pulse duration, the surface of the sample experiences maximal pressure from the plasma flow, which causes a fairly strong disturbance of the surface.

In addition to the mechanical pressure force from the plasma flow, the surface disturbance is also affected by the duration of the existence of the melt (τ). With a short duration of the existence of the melt, hydrodynamic instabilities on the alloy surface have no time to develop sufficiently and increase their amplitude. For the formation of a developed relief, a long lifetime of the melt is required, which is realized at high values of absorbed energy density. The existence of a molten state of the zirconium samples surface after exposure to CPF is confirmed by the results of solving the thermal conductivity equation with the initial and boundary conditions that determine the pulsed nature of surface heating by an external heat flow [22].

The spatial profiles of the temperature distribution over depth in the near-surface layer of irradiated zirconium caused by its pulsed heating with different absorbed energy densities at a pulse duration of 100 μs are given in Fig. 3. It can be seen that the melting of the zirconium surface layer begins at an absorbed energy density of 10–11 J/cm^2. The horizontal sections on the temperature distribution curves refer to the region of the coexistence of the melt and the solid state at the melting point. At an absorbed energy density of 30 J/cm^2, an intense process of the material evaporation begins owing to its boiling. Thus, the performed calculations made it possible to determine the optimal range of the absorbed energy density of the compression plasma flow necessary to achieve the liquid-phase mixing regime.

The results obtained (Table 1) show that, with an increase in the absorbed energy density from 15 to 35 J/cm^2, the lifetime of the melt increases from 40 to 310 μs, which increases the probability of the development of surface hydrodynamic instabilities. With a further increase in energy density, the effect of evaporation and boiling of the surface begins to take place, which does not allow us to estimate adequately the lifetime of the melt using the model applied.

In this work, zirconium samples with a preliminary chromium coating were exposed to CPF. Since the coating thickness did not exceed 1 μm, its influence on the temperature distribution and melt depth can be neglected. The spatial profiles of chromium distribu-

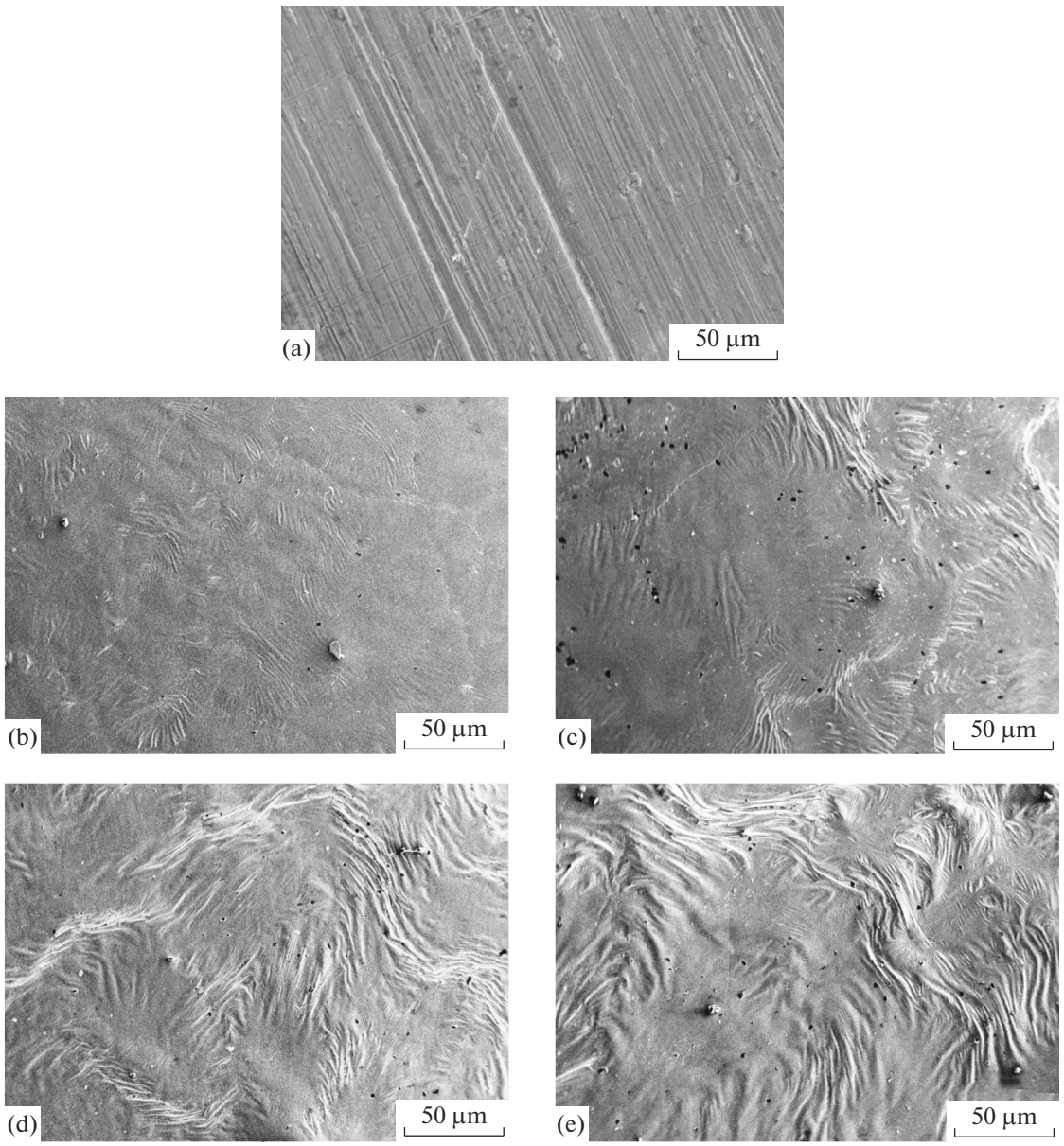

Fig. 2. SEM image of the zirconium surface in the initial state (a) and after the compression plasma flows impact at Q, J/cm^2: 25 (b), 30 (c), 37 (d), 43 (e).

tion over depth are given in Fig. 4. It can be seen that the original chromium coating has a thickness of about 0.8–0.9 μm. The chromium concentration value of 53–55 at % is associated with a fairly large area of generation of characteristic X-ray radiation of chromium atoms during measurements, which reaches 1 μm. As a result, when determining the chromium concentration distribution profile, signals from the underlying zirconium substrate simultaneously reach the detector, thereby reducing the chromium concentration. No other impurities were found in the coating.

After exposure to the CPF at an absorbed energy density of 25 J/cm^2, leading to the melting of the Cr coating and a part of the zirconium substrate, a redistribution of metals occurs in the near-surface layer. Owing to the accelerated thermal diffusion, as well as the liquid-phase mixing of two melted metals with each other, the profile of the spatial distribution of chromium has the form shown in Fig. 4b. It can be seen that the depth of its penetration reaches 4–5 μm. The same depth of the molten layer was obtained by analyzing temperature profiles (Fig. 3) at Q = 25 J/cm^2. The concentration of Cr directly on the surface is 3.0–3.5 at %. As the absorbed energy density increases, it begins to influence the process of the chromium coating evaporation, and its concentration in the modified

zirconium layer is 1.0 at % at $Q = 30$ J/cm^2 and drops to almost zero at $Q = 43$ J/cm^2.

By means of X-ray diffraction analysis, it was demonstrated that the polycrystalline structure of the modified zirconium layer is preserved after crystallization. In the initial state, only a low-temperature α phase with a hexagonal structure was detected in zirconium samples. The presence of chromium atoms in the surface layer of plasma-modified samples made it possible to stabilize the high-temperature β phase of cubic zirconium in the form of a β-Zr(Cr) solid solution (Fig. 5). According to data [23], chromium is one of the elements that can stabilize the high-temperature phase of zirconium at room temperature. The ratio of intensities of the α-Zr and β-Zr diffraction lines in the obtained diffraction patterns allows us to conclude that the ratio of their volume fractions depends on the absorbed energy density. Indeed, the maximum amount of solid solution is recorded in samples exposed to CPF at an absorbed energy density of 25 J/cm^2, at which the average chromium concentration in the layer is 2.0 at %. With an increase in the absorbed energy density to 30 J/cm^2, the average concentration of chromium in the surface layer decreases to 1.0 at %, thereby reducing the content of the β phase of zirconium. With a further increase in the absorbed energy density, the chromium concentration drops below 0.5 at % and it becomes insufficient to stabilize the high-temperature phase.

A feature of the diffraction lines of the β-Zr(Cr) solid solution is their fairly large width at half-maximum, which may indicate dispersed precipitations of the solid solution and a fairly high level of microstresses in it. In this case, this type of diffraction maximum may be associated with the inhomogeneous distribution of chromium in the solid solution, which is confirmed by the profile of its depth distribution (Fig. 4). However, the average lattice parameter of the β-Zr(Cr) solid solution was 0.3567 nm. The resulting value of the average lattice parameter is lower than that of the undoped β phase of zirconium—0.361 nm. Its decrease may be related to the size effect during the formation of the substitution type solid solution. Since the zirconium atomic radius is 160 pm, and that of chromium is 127 pm, this allows us to conclude that the average lattice parameter in the solid solution decreases.

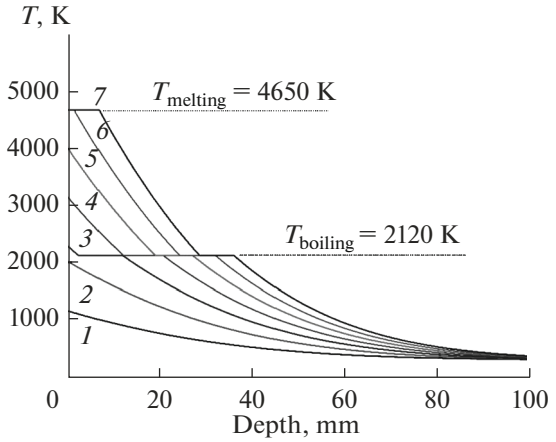

Fig. 3. Temperature profiles in the top layer of zirconium after the impact of one pulse of the compression plasma flows at Q, J/cm^2: (*1*) 5, (*2*) 10, (*3*) 15, (*4*) 20, (*5*) 25, (*6*) 30, (*7*) 35.

The main phase detected by X-ray diffraction analysis in the modified zirconium samples is the low-temperature hexagonal α phase. It should be noted that the diffraction maxima corresponding to this phase have a clear asymmetry, especially for those samples in which the β phase is detected (exposed to CPF at $Q = 25$–30 J/cm^2). Mathematical expansion of such asymmetric maxima using the Gaussian function made it possible to detect two different phases with hexagonal lattices and different parameters (Fig. 6). Indeed, experimentally recorded asymmetric lines represent a superposition of diffraction lines of fairly high intensity, from which additional lines of weak intensity are located on the side of small diffraction angles. Diffraction lines at large diffraction angles correspond to a zirconium phase with a hexagonal structure and lattice parameters $a = 0.3221$ nm and $c = 0.5134$ nm, while low-intensity diffraction lines at small diffraction angles characterize a hexagonal structure with increased values of $a = 0$ .3249 nm and $c = 0.5190$ nm. It is important to note that, in zirco-

Table 1. Parameters of existence of the zirconium melt at pulsed action of the compression plasma flows

Density of absorbed energy, Q, J/cm^2	Time from the beginning of pulse action, μs		Bplifetime of the melt, τ, μs
	up to the beginning of surface melting	up to complete crystallization of melt	
15	70	110	40
20	40	145	105
25	30	190	160
30	20	250	230
35	15	325	310

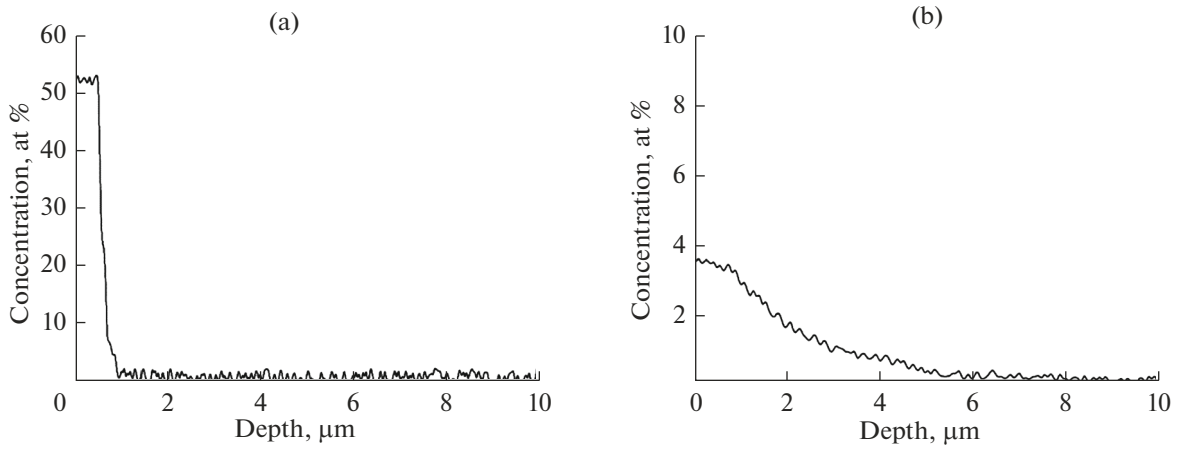

Fig. 4. Chromium concentration profiles over the depth in the initial state (a) and after the impact of compression plasma flows at $Q = 25$ J/cm^2 (b).

nium samples in which solid solution based on a high-temperature β phase was absent, only one hexagonal phase with $a = 0.3229$ nm and $c = 0.5114$ nm was detected. Taking into account that the equilibrium lattice parameters of zirconium are equal to $a_0 = 0.3231$ nm and $c_0 = 0.5146$ nm, respectively, the hexagonal phase with reduced lattice parameters represents the phase of undoped zirconium (α-Zr), formed as a result of high-speed crystallization and supersaturated with hardening vacancies. At the same time, reduction in the value of the lattice parameter can indicate a slight dissolution of chromium in hexagonal zirconium lattice with the formation of α-Zr(Cr) solid solution.

The hexagonal phase accompanying the β phase of zirconium has increased lattice parameters compared to the equilibrium ones. It can be assumed that it is a transitional phase between the high temperature and low temperature zirconium phases and is formed as the interstitial type solid solution—martensitic α'-Zr phase. As the main interstitial impurities in the martensitic phase, it is necessary to take into account both specially introduced chromium atoms and random undersized impurities introduced into the crystal lattice, which can be considered, first of all, atoms of oxygen, carbon, and nitrogen and which are adsorbed by the surface during plasma treatment. It should be expected that the depth of such impurities localization corresponds to a very thin near-surface layer, which is significantly less than the depth of the layer analyzed using X-ray radiation.

Hafnium is the most important accompanying impurity in a zirconium alloy. Elemental analysis of the surface layer showed that the hafnium concentration is practically unchanged after plasma exposure, and since the crystal lattice parameters of the alloy are compared with the corresponding parameters of zirconium in the initial state, the predominant influence

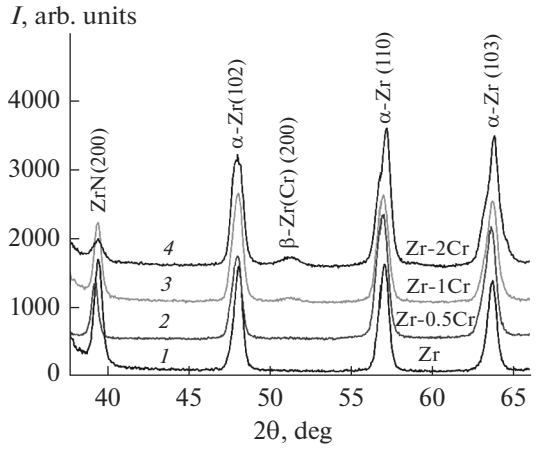

Fig. 5. XRD patterns of the zirconium after the impact of compression plasma flows at Q, J/cm^2: (*1*) 43, (*2*) 37, (*3*) 30, (*4*) 43.

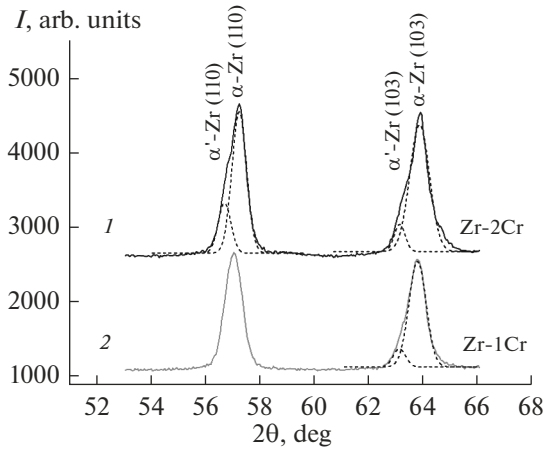

Fig. 6. XRD profile for the α-Zr after the impact of compression plasma flows at Q, J/cm^2: (*1*) 25, (*2*) 30.

of alloying chromium atoms on the change in lattice parameters can be assumed.

Structure and Phase Composition of the Zirconium–Chromium System after Isothermal Annealing

Annealing of zirconium samples in air leads to the diffusion saturation of near-surface layers with oxygen and the formation of oxide phases. In addition to oxygen from the air atmosphere, saturation with nitrogen atoms can occur, but the results of X-ray diffraction analysis showed the absence of additional nitriding, so this effect was excluded from consideration.

According to the Zr–O equilibrium phase diagram [24], at a temperature of 700°C, the initial stage of saturation with oxygen is accompanied by the formation of the α-Zr(O) solid solution, from which crystals of zirconium oxide ZrO_2 begin to precipitate at an oxygen concentration of 28–29 at %. Complete transformation of the solid solution into the oxide phase occurs at an oxygen content of 66 at %.

As is well known [25], zirconium oxide ZrO_2 can exist in three main structural modifications, differing in the type of crystal structure: monoclinic phase (*m*-ZrO_2), tetragonal phase (*t*-ZrO_2), and cubic phase (*c*-ZrO_2). The tetragonal and cubic phases are the high-temperature ones and can be stabilized at room temperature by alloying elements or residual internal stresses.

The results of X-ray diffraction analysis showed (Fig. 7a) that, already 5 min after annealing of unirradiated zirconium samples at a temperature of 700°C, growth of the *m*-ZrO_2 monoclinic phase of zirconium oxide takes place. With an increase in the diffusion time to 15 min, the intensity of the diffraction lines corresponding to the oxide phase increases, indicating an increase in its volumetric content, that is, the thickness of the oxide layer.

The results of the phase composition analysis of zirconium samples modified with chromium and subjected to plasma exposure after annealing at a temperature of 700°C are presented in Figs. 7b and 7c. The absorbed energy density was 25 J/cm^2 (maximum chromium content of 2 at %) and 43 J/cm^2 (without chromium atoms). Since the depth distribution of chromium in the modified layer (Fig. 4) is uneven, annealing at a temperature of 700°C leads to homogenization of its composition and as a result to the local chromium concentration decreasing (that is, it becomes below the critical value), and complete decomposition of the β-Zr(Cr) solid solution occurs during the first 5 min of annealing. Also, upon annealing, the asymmetry of the diffraction maxima of the low-temperature zirconium phase disappears, indicating decomposition of the nonequilibrium α'-Zr phase, which is also associated with its depletion in chromium atoms.

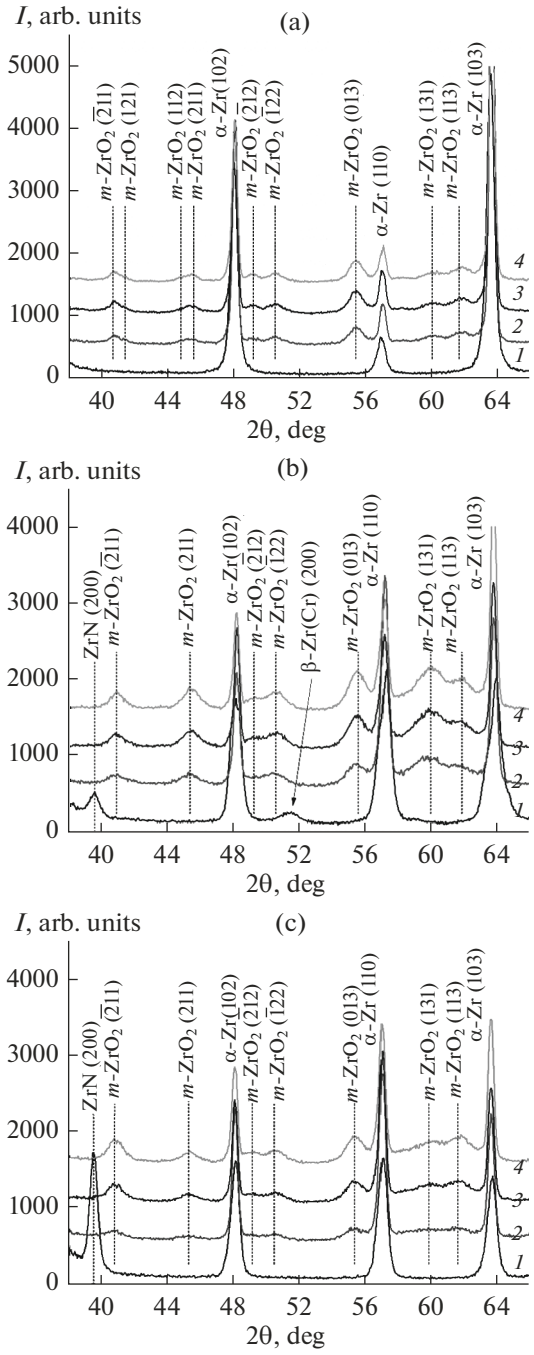

Fig. 7. XRD patterns of zirconium samples after oxidation at a temperature of 700°C: (a) initial; (b, c) after the impact of compression plasma flows at Q = 25 J/cm^2 and Q = 43 J/cm^2, respectively. (*1–4*) Exposure time of 0, 5, 10, and 15 min, respectively.

Calculation of the lattice parameters of zirconium subjected to high-temperature annealing showed that the lattice is practically undeformed in relation to the equilibrium values: the parameters of the hexagonal zirconium lattice are equal to a = 0.3228–0.3230 nm, c = 0.5143–0.5145 nm, and are practically indepen-

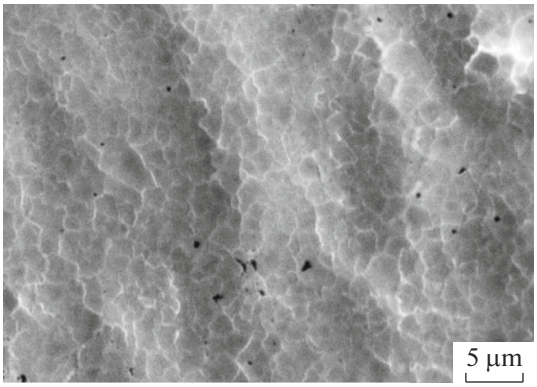

Fig. 8. SEM image of the grain structure on the surface of the zirconium after the impact of compression plasma flows with the maximum absorbed energy density of 43 J/cm^2.

dent of the annealing time. This may indicate the absence of the α-Zr(O) solid solution in the surface layer after oxidation.

Attention should be paid to the relative intensity of the diffraction lines corresponding to zirconium oxide ZrO_2, which indicates its content in the detected layer. Analysis of the initial stage of oxidation (during the first five minutes) showed a lower content of the volume fraction of the oxide phase in the zirconium sample exposed to CPF, in which the formation of the solid solution based on the high-temperature β phase of zirconium did not occur. The samples in which the β-Zr(Cr) solid solution was found were oxidized much faster. That is, during the initial stage of oxidation, oxygen diffusion predominantly occurs within crystallites of the β phase of zirconium, which have a less densely packed bcc lattice. After 5 min of oxidation, decomposition of the β-Zr(Cr) solid solution takes place, from which chromium atoms are released, and owing to their deficiency, the zirconium structure is transformed into a low-temperature hexagonal phase. The penetration of oxygen atoms into the lattice of the solid solution also deforms it, accelerating the process of its decomposition. At the following stages of annealing, oxygen diffusion occurs through the low-temperature zirconium phase and no significant difference in the intensities of ZrO_2 diffraction lines is observed.

Zirconium samples irradiated with CPF with a maximum absorbed energy density of 43 J/cm^2 are characterized by a slower process of the oxygen diffusion saturation during the annealing process. In this case, the structure of the modified layer is represented exclusively by a low-temperature zirconium phase with a hexagonal close-packed crystalline lattice. These samples showed higher resistance to oxidation at the initial stages, even compared to zirconium samples that were in the initial, unirradiated state. Most likely, this is influenced by changes in the grain structure that occur during plasma treatment. Thus, high-speed heating of the surface layer of zirconium by a plasma flow has a pulsed nature, which leads to rapid cooling and quenching from the melt, resulting in the formation of a fine-crystalline structure with an average grain size of no more than 2 μm (Fig. 8).

In addition to the grain structure and the solid solution formation, the kinetics of the zirconium high-temperature oxidation is influenced by the presence of a near-surface layer of ZrN nitride, the formation of which also takes place during exposure to CPF. At the stage of the sample cooling after the end of the plasma pulse, it interacts with the residual atmosphere consisting of a plasma-forming substance. The results of X-ray diffraction analysis clearly demonstrate the formation of the cubic zirconium nitride ZrN phase with the fcc structure, and the thickness of its layer, which determines the intensity of the corresponding diffraction lines, strongly depends on the density of absorbed energy. The maximum ZrN content is observed when exposed to a CPF with $Q_{max} = 43$ J/cm^2, while its decrease to 25 J/cm^2 leads to a decrease in the nitride fraction in the surface layer. In [26], using the example of titanium and low-carbon steel, the opposite regularity was established—with increasing absorbed energy density, the volume fraction of the nitride phase decreases. This can be explained by the surface diffusion saturation with nitrogen during the cooling of the crystallized layer, which is slowed down by the shock-compressed layer formed in the immediate vicinity of the surface during the interaction of the plasma flow with the target surface. As the absorbed energy density increases, the lifetime of such a layer increases, reducing the duration of nitrogen diffusion. This leads to a decrease in the nitrogen concentration and the thickness of the nitrided zirconium layer at high densities of absorbed energy. The observed regularity in the case of the Zr–Cr alloy of increase in the zirconium nitride volume with increasing absorbed energy density may be associated with the presence of additional chromium atoms in the surface layer. And since chromium has a low chemical affinity for nitrogen, the formation of nitrogen-containing phases based on it is difficult.

Thus, the formed zirconium nitride ZrN acts as a barrier layer for the diffusion penetration of oxygen at the initial stages of the oxidation process. After the first five minutes of annealing at a temperature of 700°C, ZrN completely decomposes and oxygen diffusion is accelerated. Influence of the absorbed energy density and chromium concentration in a modified zirconium layer on the kinetics of its oxidation is confirmed by the results of X-ray spectral microanalysis carried out on transverse sections of samples (Fig. 9). The results show that the oxygen concentration profile forms a horizontal plateau after annealing for 15 min at the level of values 55–70 at %, which corresponds to the formation of zirconium oxide ZrO_2, the stoichio-

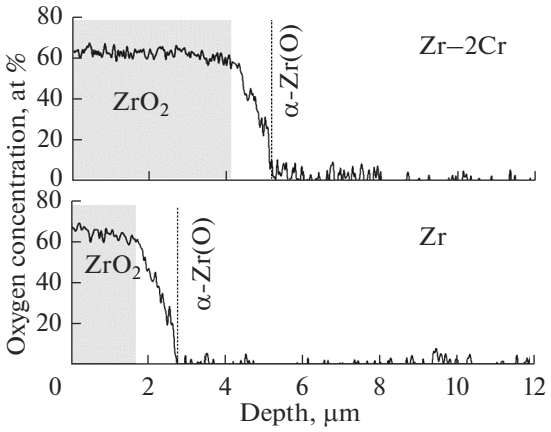

Fig. 9. Oxygen concentration profile over the depth in Zr–2Cr and Zr after oxidation at the temperature of 700°C for 15 min.

metric composition of which is close to the experimentally detected oxygen concentration. Note that the thickness of the oxide layer was about 4.0 μm for the zirconium sample containing the high-temperature (Zr–2Cr alloy) phase and did not exceed 2.0 μm for the single-phase zirconium samples. A layer of zirconium oxide is clearly detected on the surface of the samples under study in the course of investigation of the transverse sections by scanning electron microscopy (Fig. 10). Below the ZrO_2 oxide layer, the oxygen concentration drops sharply to zero, forming a narrow transition region in which the α-Zr(O) solid solution is seemingly localized. The thickness of the layer in which the α-Zr(O) solid solution is present is about 1.0 μm and does not depend on the elemental composition of the modified surface layer.

High-temperature oxidation of zirconium leads to an increase in the mass of samples, which is explained by the introduction of oxygen into the surface layer due to diffusion solid-phase saturation (Fig. 11). The characteristic dependences of the increase in sample mass have a parabolic form, indicating the predominance of the diffusion mechanism of mass transfer. Samples exposed to CPF with an absorbed energy density of 25 J/cm^2 with the subsequent formation of the β-Zr(Cr) solid solution with a bcc structure are oxidized at the highest rate, and the increase in mass of the sample after annealing for 15 min is almost twice as high as the corresponding increase in mass of the original zirconium sample. Samples of modified zirconium at a maximum energy density of 43 J/cm^2, when both chromium and the β-Zr(Cr) solid solution are absent in the surface layer, are characterized by a minimal increase in mass, which is two times less than that of the original zirconium sample. The results obtained are in complete agreement with the oxygen concentration profiles and the results of X-ray diffraction analysis.

CONCLUSIONS

The possibility of doping a near-surface layer of zirconium with chromium atoms from a pre-deposited thin (1 μm) chromium coating when the coating is exposed to a compression plasma flow with an absorbed energy density of 25–43 J/cm^2 has been demonstrated. As a result, the high-temperature β phase of zirconium is stabilized in the form of the β-Zr(Cr) solid solution when the average chromium concentration in the alloyed layer exceeds 1 at %. The formation of the β-Zr(Cr) solid solution is accompanied by the formation of an intermediate martensitic phase α'-Zr in the form of chromium supersaturated solid solution in the low-temperature hexagonal phase of zirconium.

The high-temperature zirconium phase that appears in the modified layer accelerates its diffusion saturation with oxygen under conditions of isothermal annealing at atmospheric pressure and at a temperature of 700°C. During the first 15 min of oxidation, a layer of monoclinic zirconium oxide 4 μm thick is formed on the surface. The thickness of the oxide layer

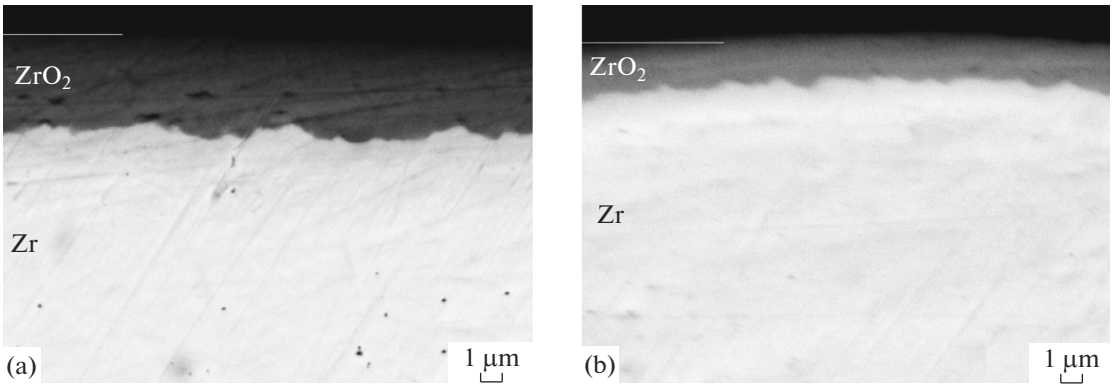

Fig. 10. SEM image of the cross section of the oxidized Zr–2Cr (a) and Zr (b) samples after oxidation at the temperature of 700°C for 15 min.

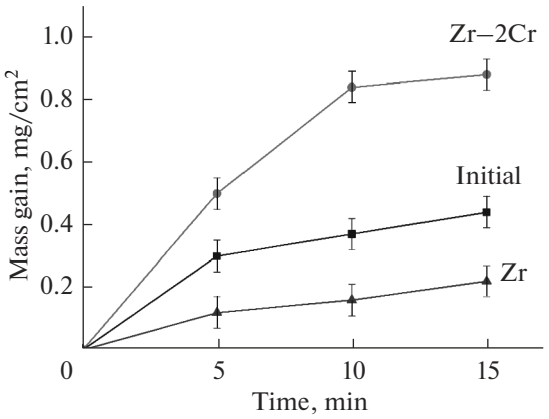

Fig. 11. The mass gain of the zirconium samples after oxidation at the temperature of 700°C.

is reduced to 2 μm in the absence of the solid solution based on the β-zirconium phase in the modified layer. Zirconium samples modified by a compression plasma flow at a maximum absorbed energy density of 43 J/cm^2, when the effect of alloying the surface layer with chromium atoms is absent owing to its intense evaporation and ablation at the stage of surface heating by the plasma flow, are characterized by increased resistance to high-temperature oxidation at its initial stages compared to the initial state.

FUNDING

This work was supported by ongoing institutional funding. No additional grants to carry out or direct this particular research were obtained.

CONFLICT OF INTEREST

The authors of this work declare that they have no conflicts of interest.

REFERENCES

1. Yakushkin, A.A., On the problems of creating shells of fuel rods from zirconium alloys for tolerant fuel, *Fiz. Khim. Obrab. Mater.,* 2021, no. 3, pp. 69–78. https://doi.org/10.30791/0015-3214-2021-3-69-78
2. Kritskii, V.G., Motkova, E.A., and Yashin, A.S., A model of the relationship between the oxidation parameters of zirconium alloys in water steam at 1000°C and the alloy composition. I. Data analysis and model development, *Fiz. Khim. Obrab. Mater.,* 2020, no. 2, pp. 58–64. https://doi.org/10.30791/0015-3214-2020-2-58-64
3. Kritsky, V.G., Motkova, E.A., and Yashin, A.S., A model of the relationship between the parameters of oxidation of zirconium alloys in water steam at 1000°C and the alloy composition: II. Model selection, comparison with experiment, *Inorg. Mater.: Appl. Res.,* 2021, vol. 12, no. 3, pp. 700–706. https://doi.org/10.1134/S2075113321030217
4. Nikulin, S.A., Rozhnov, A.B., Belov, V.A., Li, E.V., and Koteneva, M.V., Kinetics of high-temperature oxidation and embrittlement factors of zirconium alloys in tests simulating LOCA-type accidents in nuclear power plants, *Prot. Met. Phys. Chem. Surf.,* 2012, vol. 48, no. 1, pp. 97–105. https://doi.org/10.1134/S2070205112010108
5. Thieurmal, R., Besson, J., Pouillier, E., Parrot, A., Ambard, A., and Gourgues-Lorenzon, A.-F., Contribution to the understanding of brittle fracture conditions of zirconium alloy fuel cladding tubes during LOCA transient, *J. Nucl. Mater.,* 2019, vol. 527, p. 151815. https://doi.org/10.1016/j.jnucmat.2019.151815
6. Hazan, J., Gauthier, A., Pouillier, E., and Shirvan, K., Semi-integral LOCA test of cold-spray chromium coated zircaloy-4 accident tolerant fuel cladding, *J. Nucl. Mater.,* 2021, vol. 550, p. 152940. https://doi.org/10.1016/j.jnucmat.2021.152940
7. Ivanov, A.V., Kuraev, A.Yu., Malakhov, A.A., Lerner, A.E., and Luzan, Yu.V., The study properties of protective chrome coating on the samples-simulators of WWER fuel rods, *Vopr. At. Nauki Tekh., Ser.: Materialoved. Nov. Mater.*, 2018, no. 3 (94), pp. 116–130.
8. Berlin, E.V., Grigor'ev, V.Yu., Ivanov, A.V., Isaenkova, M.G., Klyukova, K.E., and Stolbov, S.D., Structure of the protective chromium coating obtained by a thermal evaporation method in a magnetron discharge on the cladding tube from E110 alloy, *Tsvetn. Met.,* 2019, no. 4, pp. 33–40. https://doi.org/10.17580/tsm.2019.04.04
9. Isaenkova, M.G., Perlovich, Yu.A., Stolbov, S.D., Klyukova, K.E., Fesenko, V.A., and Berlin, E.V., Influence of technology of obtaining chromium coating on cladding tubes from 1%Nb–(O, Fe) alloy on change of its structure during air oxidation at temperatures 400–1150°C, *Tsvetn. Met.,* 2020, no. 2, pp. 68–77. https://doi.org/10.17580/tsm.2020.02.09
10. Tian, X.B., Jiang, H.F., Yang, S.Q., Luo, Z.J., Fu, R.K.Y., and Chu, P.K., Plasma processing of AISI 304 stainless steel using radio frequency hollow cathode discharge, *Surf. Coat. Technol.,* 2007, vol. 201, pp. 8650–8653. https://doi.org/10.1016/j.surfcoat.2006.01.077
11. Sartowska, B., Piekoszewski, J., Walis, L., Senatorski, J., Stanislawski, J., Ratajczak, R., Nowicki, L., Kopcewicz, M., Prokert, F., and Barlak, M., Structural and tribological properties of carbon steels modified by plasma pulses containing inert and active ions, *Surf. Coat. Technol.,* 2007, vol. 201, pp. 8295–8297. https://doi.org/10.1016/j.surfcoat.2006.01.088
12. Hassan, M., Ahmad, R., Qayyum, A., Murtaza, G., Waheed, A., and Zakaullah, M., Surface modification of AlFe1.8Zn0.8 alloy by using dense plasma focus, *Vacuum,* 2006, vol. 81, pp. 291–298. https://doi.org/10.1016/j.vacuum.2006.05.001
13. Paikin, A.G., Shulov, V.A., Krainikov, A.V., Teryaev, A.D., Remnev, G.E., and Engel'ko, V.I., Promising surface treatment technologies in the manufacture and repair of GTE blades made of titanium alloys using high-power ion and high-current electron beams, *Fiz. Khim. Obrab. Mater.,* 2007, no. 3, pp. 44–56.

14. Rotshtein, V.P., Markov, A.B., Shevchenko, N., Reuther, H., Oskomov, K.V., and Shulov, V.A., Surface doping of VT6 alloy with zirconium by pulsed electron-beam mixing of predeposited multilayer Zr/Ti film, *Tech. Phys. Lett.,* 2008, vol. 34, no. 10, pp. 891–894. https://doi.org/10.1134/S1063785008100246
15. Shepel', D.A. and Markov, A.B., Low energy high current electron beam heating of target with second phase microinclusions, *Tech. Phys. Lett.,* 2011, vol. 37, no. 8, pp. 772–775. https://doi.org/10.1134/S1063785011080256
16. Cherenda, N.N., Uglov, V.V., Anishchik, V.M., Stalmashonak, A.K., Astashinski, V.M., Kuzmickii, A.M., Punko, A.V., Thorwath, G., and Stritzker, B., Modification of high-speed steels by nitrogen compression plasma flow: Structure, element composition, tribological properties, *Surf. Coat. Technol.*, 2006, vol. 200, pp. 5334–5342. https://doi.org/10.1016/j.surfcoat.2005.06.007
17. Astashynski, V.M., Ananin, S.I., Kostyukevich, E.A., Kuzmitski, A.M., Uglov, V.V., Anishchik, V.M., Cherenda, N.N., Stalmashonak, A.K., and Sveshnikov, Yu.V., Comprehensive modification of semiconductors and metals providing new structural features of surface layers subjected to compression plasma flows, *J. High Temp. Mater. Process.,* 2007, vol. 11, no. 4, pp. 536–548. https://doi.org/10.1016/j.surfcoat.2005.02.079
18. Uglov, V.V., Anishchik, V.M., Cherenda, N.N., Stal'moshenok, E.K., Astashinskii, V.M., and Kuz'mitskii, A.M., Structure and phase condition of the system of titanium-steel irradiated with nitrogen compressed plasma flow, *Fiz. Khim. Obrab. Mater.,* 2005, no. 2, pp. 36–41.
19. Yakushkin, A.A., Borisov, V.M., and Trofimov, V.N., Properties of chromium coatings applied by various methods to zirconium alloy E110, *Inorg. Mater.: Appl. Res.,* 2022, vol. 13, no. 3, pp. 721–727. https://doi.org/10.1134/S2075113322030406
20. Kashkarov, E.B., Sidelev, D.V., Syrtanov, M.S., Tang, C., and Steinbrück, M., Oxidation kinetics of Cr-coated zirconium alloy: Effect of coating thickness and microstructure, *Corros. Sci.,* 2020, no. 175, p. 108883. https://doi.org/10.1016/j.corsci.2020.108883
21. Wang, X., Guan, H., Liao, Y., Zhu, M., Xu, C., Jin, X., Liao, B., Xue, W., Zhang, Y., Bai, G., and Wang, R., Enhancement of high temperature steam oxidation resistance of Zr–1Nb alloy with ZrO_2/Cr bilayer coating, *Corros. Sci.,* 2021, vol. 187, p. 109494. https://doi.org/10.1016/J.CORSCI.2021.109494
22. Uglov, V.V., Shimanskii, V.I., Cherenda, N.N., Astashinskii, V.M., and Kvasov, N.T., Convective mass transfer in the surface Ti layers after the action of compression plasma fluxes, *Fiz. Khim. Obrab. Mater.,* 2012, no. 6, pp. 31–39.
23. Chen, K., Zeng, L., Li, Z., Chai, L., Wang, Y., Chen, L., and Yu, H., Effects of laser surface alloying with Cr on microstructure and hardness of commercial purity Zr, *J. Alloys Compd.,* 2019, vol. 784, pp. 1106–1112. https://doi.org/10.1016/j.jallcom.2019.01.097
24. *Diagrammy sostoyaniya dvoinykh metallicheskikh sistem: Spravochnik* (Phase Diagrams of Binary Metallic Systems: Handbook), Lyakishev, N.P., Ed., Moscow: Mashinostroenie, 2001, vol. 3, book 1.
25. Fedorov, P.P. and Yarotskaya, E.G., Zirconium dioxide. Review, *Kondens. Sredy Mezhfaznye Granitsy*, 2021, vol. 23, no. 2, pp. 169–187. https://doi.org/10.17308/kcmf.2021.23/3427
26. Cherenda, N.N., Shimanskii, V.I., Uglov, V.V., Astashinskii, V.M., and Ukhov, V.A., Nitriding of steel and titanium surface layers under the action of compression plasma flows, *J. Surf. Invest.: X-Ray, Synchrotron Neutron Tech.*, 2012, vol. 6, no. 2, pp. 319–325. https://doi.org/10.1134/S1027451012040088

Translated by N. Rukk